

Reactive ion etching of quartz and Pyrex for microelectronic applications

D. A. Zeze, R. D. Forrest, J. D. Carey, D. C. Cox, I. D. Robertson, B. L. Weiss, and S. R. P. Silva

Citation: *Journal of Applied Physics* **92**, 3624 (2002);

View online: <https://doi.org/10.1063/1.1503167>

View Table of Contents: <http://aip.scitation.org/toc/jap/92/7>

Published by the [American Institute of Physics](#)

Articles you may be interested in

[Plasma etching of Si and SiO₂—The effect of oxygen additions to CF₄ plasmas](#)

Journal of Applied Physics **49**, 3796 (2008); 10.1063/1.325382

[Smooth surface glass etching by deep reactive ion etching with SF₆ and Xe gases](#)

Journal of Vacuum Science & Technology B: Microelectronics and Nanometer Structures Processing, Measurement, and Phenomena **21**, 2545 (2003); 10.1116/1.1624272

[Anisotropic etching of SiO₂ in low-frequency CF₄/O₂ and NF₃/Ar plasmas](#)

Journal of Applied Physics **55**, 242 (1998); 10.1063/1.332872

[Spectroscopic diagnostics of CF₄-O₂ plasmas during Si and SiO₂ etching processes](#)

Journal of Applied Physics **52**, 1259 (1998); 10.1063/1.329748

[Chemical dry etching of silicon nitride and silicon dioxide using CF₄/O₂/N₂ gas mixtures](#)

Journal of Vacuum Science & Technology A: Vacuum, Surfaces, and Films **14**, 2802 (1998); 10.1116/1.580203

[Reactive ion etching of piezoelectric materials in CF₄/CHF₃ plasmas](#)

Journal of Vacuum Science & Technology A: Vacuum, Surfaces, and Films **16**, 2037 (1998); 10.1116/1.581307

Scilight

Sharp, quick summaries **illuminating**
the latest physics research

Sign up for **FREE!**



Reactive ion etching of quartz and Pyrex for microelectronic applications

D. A. Zeze,^{a)} R. D. Forrest, J. D. Carey, D. C. Cox, I. D. Robertson, B. L. Weiss,
and S. R. P. Silva

*School of Electronics, Computing and Mathematics, University of Surrey, Guildford GU2 7XH,
United Kingdom*

(Received 28 March 2002; accepted for publication 1 July 2002)

The reactive ion etching of quartz and Pyrex substrates was carried out using CF_4/Ar and CF_4/O_2 gas mixtures in a combined radio frequency (rf)/microwave (μw) plasma. It was observed that the etch rate and the surface morphology of the etched regions depended on the gas mixture (CF_4/Ar or CF_4/O_2), the relative concentration of CF_4 in the gas mixture, the rf power (and the associated self-induced bias) and microwave power. An etch rate of 95 nm/min for quartz was achieved. For samples covered with a thin metal layer, *ex situ* high resolution scanning electron microscopy and atomic force microscopy imaging indicated that, during etching, surface roughness is produced on the surface beneath the thin metallic mask. Near vertical sidewalls with a taper angle greater than 80° and smooth etched surfaces at the nanometric scale were fabricated by carefully controlling the etching parameters and the masking technique. A simulation of the electrostatic field distribution was carried out to understand the etching process using these masks for the fabrication of high definition features. © 2002 American Institute of Physics. [DOI: 10.1063/1.1503167]

I. INTRODUCTION

The microfabrication of glass structures using plasma etching is a promising emerging technology which can be used in a variety of areas, such as optoelectronics, millimeter-wave technology, microelectromechanical systems (MEMS), capillary chips and diffraction gratings.¹ Because glass is a relatively cheap suitable substrate for good ion-exchange waveguides, it is often used in integrated optics devices. For integrated sensors,² the ability to fabricate structures with near vertical sidewalls and reduced surface roughness is a key factor. In this regard, the control of surface roughness is especially important for optical and microwave devices since surface roughness can induce light scattering and signal loss which ultimately degrades device performance.³ The fabrication of suitable structures can be achieved by optimizing the etching process parameters. In addition, the range and degree of control of the process parameters offered by a particular etching system determine its suitability for a given application. For the fabrication of such high precision devices, dry etching, because of its anisotropic properties, is commonly preferred to wet etching which is generally isotropic and can induce undesirable undercutting.

Dry etching occurs when the ion and neutral species produced in a plasma discharge interact with the substrate and it can be characterized by two different processes. These are sputter etching, where the etching is due to the kinetics of the ion and neutral species produced in the plasma, and reactive ion etching (RIE), where it is the chemical reaction between the ions and the substrate that results in the etching. The etch rate, shape and morphology of the etched features are dependent on the extent to which one of these dry etch mecha-

nisms is dominant which in turn depends on the etching system and process parameters. There are a number of different types of plasma sources, such as those based on direct current discharge, radio frequency (rf) sources (capacitively coupled or inductively coupled) and microwave (μw) sources (electron cyclotron resonance, surfatron, etc.).⁴ In addition, in the RIE process different types of reactive gases such as CF_4 , SF_6 , CHF_3 and chlorine-based gases can be used. These reactive gases are often mixed to user-defined concentrations with argon, oxygen or hydrogen to enhance the etching properties of the plasma.

In this article we report on the etching of features in quartz and Corning 7740 (Pyrex) using a combined rf microwave etching system (rf/ μw RIE) analyzed with surface profilometry, scanning electron microscopy (SEM) and atomic force microscopy (AFM) techniques. The etch rate, surface topography, taper angle and surface roughness of the etched structures are investigated as a function of the etching parameters. We also investigate the effects of different masking techniques on the etched features. The simulation of the edge profile indicates how masking can be modified to achieve the required well-defined device structures.

II. EXPERIMENT

The rf/ μw RIE system was designed to be able to both deposit thin films by plasma enhanced chemical vapor deposition (PECVD) and to reactively ion etch features in samples. A schematic of the system is shown in Fig. 1. The sample is placed on a 11.5 cm diameter driven electrode (sample holder). After suitable vacuum is achieved ($\sim 10^{-7}$ Torr), process gases are introduced into the chamber using mass flow controllers. The plasma is then ignited using a tunable capacitively coupled rf source powered by a ENI HF-300 supply before the μw radiation is coupled into the chamber (supplied by a magnetron powered by a Muegge

^{a)}Corresponding author; electronic mail: d.zeze@surrey.ac.uk

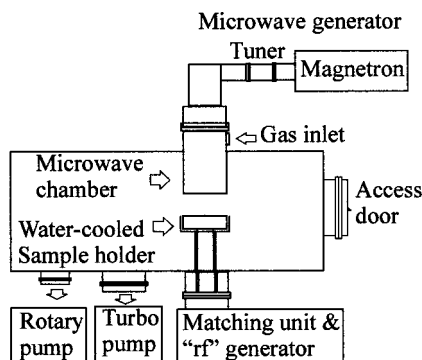


FIG. 1. Schematic of the radio frequency combined microwave reactive ion etching system.

supply). The plasma is pulled through the microwave cavity towards the sample under the influence of the negative self-bias produced on the substrate table by the rf signal. To minimize the rf and microwave reflected power during the deposition or etching process, the system is tuned using an inductive matching unit for the rf source and a longitudinal coarse and three-stud fine tuner for the microwave source.

The RIE of quartz and Pyrex samples was carried out using high purity CF_4/Ar and CF_4/O_2 gas mixtures in the rf/ μw -RIE system. The substrates (approximately 1 cm^2) used are commercially available Pyrex (borosilicate glass, Corning 7740 standard, provided by Corning International, Wiesbaden, Germany) and fused quartz [very fine (VF) grade, provided by Heraeus, Byfleet, England] which were cleaned using acetone, methanol, isopropanol and de-ionized water prior to etching. Subsequently, the mask layers were prepared by either evaporating a thin Ni metal film, patterned using standard photolithographic techniques, or by attaching a silicon wafer to the sample using vacuum adhesive pads. Prior to etching, the chamber was evacuated to a base pressure of $\sim 10^{-7}$ Torr. The microwave power levels were varied between 0 and 1200 W for the 2.45 GHz source. The rf power level was also varied between 0 and 300 W for the 13.56 MHz rf generator, corresponding to a negative self-bias of 0–500 V. In order to more efficiently control device fabrication, the system was calibrated by systematically varying the process gas flow rates, process pressure (5–60 mTorr), gas mixture and the rf and μw power levels. During the etching process, the sample holder was water cooled to keep the sample near room temperature to prevent any thermally induced effects on the sample. A K-type thermocouple was incorporated into the process chamber to monitor the sample holder temperature before and after processing.

After etching any remaining mask material was removed by wet chemical etching. The processed samples were analyzed using a surface profilometer (Sloan Technology Dektak IIA) with resolution better than 1 nm to measure the etch depth. A Hitachi S4000 cold field emission gun SEM operating at 5 kV was used to study the surface morphology of the specimens and secondary electron signals were used to evaluate the etch profiles. Ambient AFM measurements were performed using a Digital Instruments Nanoscope IIIA operating in tapping mode to quantitatively evaluate the etch profile and surface roughness.

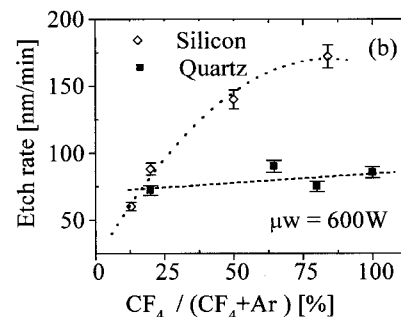
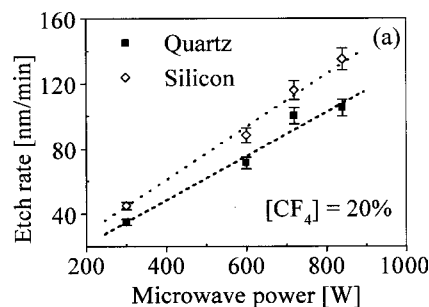


FIG. 2. Etch rate of fused quartz and silicon $\langle 100 \rangle$ as a function of the microwave power at 20% CF_4 in the chamber (a) and CF_4 composition in the gas mixture for a microwave power of 600 W (b).

III. RESULTS AND DISCUSSION

A. Etch rate and system calibration

An initial calibration of the rf/ μw -RIE system for a fixed microwave power of 300 W showed that 30–35 mTorr, 20% CF_4 (in Ar) and 320–400 V were the optimum values of process pressure, gas mixture and negative self-bias, respectively. These operating conditions resulted in etch rates of about 45 nm/min for a silicon wafer ($\langle 100 \rangle$, *p* type) and 30 nm/min for quartz. This latter value is similar to that reported by Leech⁵ for etching quartz in a rf CF_4 plasma with a negative self-bias voltage in the range of 320–360 V. Note that, under given processing conditions, the etch rate of Pyrex specimens was similar to that of quartz. The effects of increasing the microwave power level and the percentage of CF_4 in the gas mixture are shown in Fig. 2 for both silicon and quartz. In Fig. 2(a), the etch rates of Si and quartz are seen to increase up to 130 and 100 nm/min, respectively, as the power level is increased to 850 W. The effects of the varying the CF_4 content in the gas mixture were also investigated for a fixed microwave power of 600 W and are shown in Fig. 2(b). The etch rate of Si increases to 172 nm/min as the concentration of CF_4 in the mixture is raised to 84% and saturates thereafter, whereas the maximum etch rate of quartz, 95 nm/min, does not vary significantly as the CF_4 content in the gas mixture is varied from 0% to 100% for a constant microwave power of 600 W. For the RIE system described above, the etch rate of quartz using -340 V self-bias is 95 nm/min is more than twice that reported by Leech⁵ for similar self-bias voltages in a CF_4 rf plasma source. However, higher etch rates up to $\sim 1\ \mu\text{m}/\text{min}$, have been

achieved elsewhere⁶ using an inductively coupled plasma (ICP). The high etch rate produced by an ICP system is attributed to the greater plasma density and other parameters, such as plasma potential and ion energy spread. In an ICP system, the ion density is $>10^{11}$ ions/cm³ and can reach 10^{13} ions/cm³.^{7,8} In turn, although rf coupled systems can theoretically reach 10^{12} ions/cm³, only about 10^{10} – 10^{11} ions/cm³ are measured. In the system in this study, the etching chamber used is designed to incorporate a load lock with *in situ* scanning tunneling microscopy facilities and the volume of the entire system vessel and the microwave cavity are ~ 1 and ~ 0.01 m³, respectively. This may affect the confinement and reduce the density of the plasma. Under the same processing conditions, the etch rate for a quartz sample increased from 30 to 40 nm/min when an internal side shielding wall was inserted into the microwave cavity, thereby reducing the diameter of the cylindrical cavity from 15 to 11.5 cm.

In order to further investigate the etch rate of the rf/ μ w-RIE system, the etching characteristics of CF₄/Ar were compared with those of CF₄/O₂ gas mixtures. The results indicate that, under the same experimental conditions (power levels, gas flows, process pressure) which were optimized for CF₄/Ar, the etch rate using a CF₄/O₂ plasma is at least 1.5 times higher than that for CF₄/Ar for all the materials studied here. This is comparable to results reported elsewhere.⁹

B. Surface roughness

The Pyrex samples were masked by evaporating a thin (~ 150 nm) Ni layer and patterned using conventional photolithography. The RIE process was set up to etch 1–3 μ m, using either CF₄/O₂ or CF₄/Ar plasma to study the resultant surface roughness of the etched surfaces while all other experimental conditions were kept constant. A detailed SEM and AFM study of the etched profiles combined with the surface profilometry data was used to evaluate qualitatively and quantitatively the surface roughness and the quality of the sidewalls. SEM images of Pyrex samples etched in CF₄/O₂ and in CF₄/Ar plasma are shown in Fig. 3. On a 30 μ m scale, a comparison of Fig. 3(a) with Fig. 3(b) indicates that the masked region of the specimen etched using the CF₄/Ar [Fig. 3(b)] exhibits a higher surface roughness than the masked region subject to a CF₄/O₂ etch. The roughnesses of the etched and masked areas are very similar to those for the sample etched with the CF₄/O₂ [Fig. 3(a)] whereas the masked area of the CF₄/Ar etched sample is considerably rougher than the etched area [Fig. 3(b)]. One can also observe that the neighboring region between the etched and masked areas (interface) shows a degree of roughness that is higher than that of the etched areas. This is indicative of the difficulty of fully controlling the etching process and is believed to result from the reflections and multiple scattering of species onto the sidewall. The difference in the electrical field distribution in the regions neighboring the edges cannot be discounted either in this particular case (as discussed later). Higher magnification images (1 μ m scale) of the specimens shown in Figs. 3(c) and 3(d) underscore the difference in surface roughness for the differ-

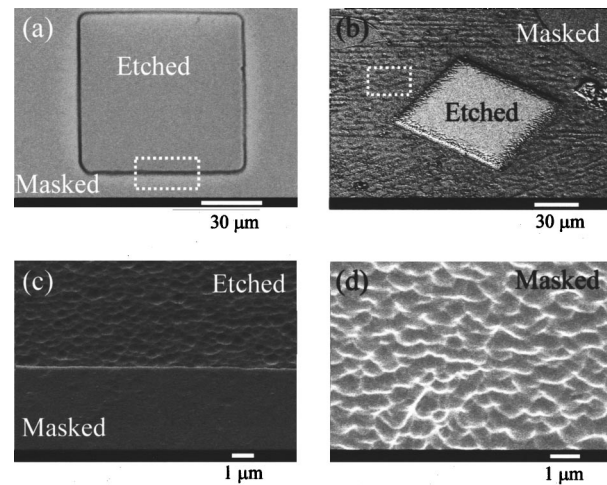


FIG. 3. SEM characteristics of Pyrex etched using a CF₄/O₂ plasma (a), (c) and a CF₄/Ar plasma (b), (d). The images are shown on 30 and 1 μ m scales for (a), (c) and (c), (d), respectively.

ent gas mixtures used. The masked (unetched) region in Fig. 3(d) exhibits an estimated surface roughness of 200 nm whereas the sample in Fig. 3(c) exhibits a smooth unetched area. The etched area in Fig. 3(c) gives a root mean square (rms) roughness ~ 50 nm from the AFM measurements shown in Table I.

The surface topography of the etched samples was studied in detail using AFM. Typical surface maps of the etched and masked areas for the sample processed with the CF₄/O₂ plasma are shown in Figs. 4(a) and 4(b), respectively. The analysis of the sample etched using CF₄/O₂ gives rms surface roughness values of 34 and 49 nm for the masked and etched surfaces of the Pyrex samples, respectively. The rms surface roughnesses of the Pyrex samples after RIE with different gas mixtures and masks are given in Table I. The results indicate that the low rms roughness of the Pyrex sample before etching (rms roughness of ~ 9 nm) is increased after etching through a thin (~ 150 nm) conventional Ni mask. It is reasonable to believe that the wet etch which removes the remaining mask material plays a role in increasing the roughness of the masked regions. However, since all the samples were processed under the same wet etching conditions, it is unlikely that the wet etch (removal) of the mask material is responsible for roughening of the surface below the mask. If it contributes to the roughening, then the contribution is expected to be similar for all the specimens regardless of the dry etching process under which they have been processed prior to wet removal of the mask material. This roughness induced below the mask that occurs in parallel

TABLE I. AFM rms surface roughness (in nm) of Pyrex substrates etched using different gas mixtures for different mask materials.

Etchant gas mixture	Mask material	Surface roughness (nm)	
		Etched	Masked
CF ₄ /O ₂	Ni	49	34
CF ₄ /Ar	Ni	50	149
CF ₄ /Ar	Si wafer	136	9

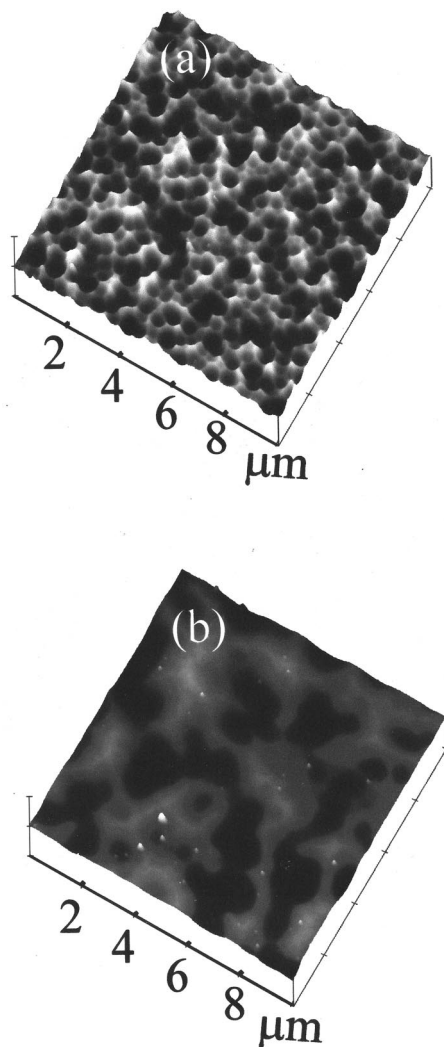


FIG. 4. AFM images of a Pyrex sample showing the rms surface roughness induced by the reactive ion etching process on the etched area (a) and beneath the masked region (b).

with the etching of the exposed areas is more pronounced using the CF_4/Ar plasma than the CF_4/O_2 plasma. Therefore, these results are thought to originate from the kinetic properties of the ion and neutral species impacting the relatively thin mask thereby producing craters in the sample below the metal mask, a purely “ballistic” or “physical sputtering effect.” Since the argon ions are much heavier than the oxygen ions, this effect is expected to be more marked in a CF_4/Ar plasma than in a CF_4/O_2 plasma, as observed.

The data in Table I also show that surface roughness values as low as 49 nm can be achieved on the etched surfaces. For 3–5 μm deep structures devices processed in the rf/ μw -RIE system, the surface rms roughness was below 150 nm. This is significantly less than the rms roughness value of 1 μm for similar features etched in Pyrex that have been reported in the literature.⁶ The rms roughness was also measured (surface profilometry and SEM) to be ~ 200 nm for 15 and 21 μm deep structures, indicating that the roughness induced using the RIE process does not scale linearly with the etch depth. This is particularly important for deep etching, such as that used for MEMS devices. For example, in

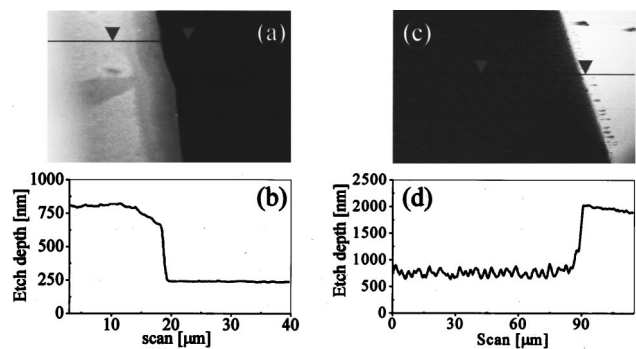


FIG. 5. Etch profiles of Pyrex for a specimen covered with a thin metal layer (a), (b) and for a specimen with a dielectric layer coating on the metal mask (c), (d).

the fabrication of multichip optoelectronic module (MOM) structures, the surface roughness plays a significant role since the level of scattering and microwave losses, which are related to the surface roughness, modify the optical and microwave properties of the structure. As reported by Berg and Pang,¹⁰ the surface damage, reflectivity, sidewall damage, defect density, thermal load etc. that occur during the etching process can degrade device characteristics. The selectivity factor of the masking materials can affect the surface roughness of the etched areas, since materials with a relatively higher etch rate will tend to result in the redeposition¹¹ of more nonvolatile materials than masks with a relatively low etch rate. For example, the etch rate of a silicon wafer is much higher than that of Ni. In our case, for the sample masked by Si, more nonvolatile materials may be redeposited onto the etched area, thereby inducing a higher degree of roughness as indicated in Table I (136 compared to ~ 50 nm for the sample coated with a nickel layer).

C. Taper angle and edge profile

Two sets of Pyrex samples (labeled S1 and S2) coated with approximately 150 nm of Ni were patterned using photolithographic techniques and AZ4330a photoresist which produces a ~ 3 μm thick film. After patterning the nickel, the resist layer was removed from sample S1 using acetone whereas for sample S2 the photoresist covering the nickel was not removed. Both samples were processed simultaneously in the RIE system using the same plasma conditions. The AFM edge profiles of these samples are shown in Fig. 5. From these profiles and the data collected from the deep etched structures (5–15 μm), the taper angle was measured to be between 80° and 86° for both samples, which is desirable for device manufacture. The taper angles obtained here are comparable to those of 79° – 88° reported in the literature.⁶ Also, for sample S2, with the photoresist coating [Fig. 5(c)], the etched area is relatively rough, with a rms value of 82 nm, compared to 49 nm for the sample without the photoresist covering the metal mask. Before removing the excess photoresist and the Ni mask, solid residues were observed on the etched areas using an optical microscope. This is probably due to nonvolatile materials being released from the photoresist and redepositing onto the surface being etched during the process as already demonstrated

elsewhere.¹² This effect of materials redepositing randomly onto the surface being etched could reduce the etch rate and induce a higher degree of roughness that compromises the uniformity of the etched surfaces.

A comparison of the pictures and scan profiles shown in Fig. 5 shows interesting differences between the profiles at the boundary between the etched and unetched regions. In Figs. 5(c) and 5(d), sample S2 (with the photoresist coating covering the Ni mask) exhibits a sharp change between the unetched surface and the etch wall, resulting in near vertical sidewalls. In contrast, in Figs. 5(a) and 5(b), sample S1, without the photoresist coating on the mask, has a graded boundary between the sidewall and masked area. This erosion of the corner, with an angle of approximately 45° in the plot, can be seen clearly in both the surface maps and the section profiles. Note that similar features with rounded corners were observed on silica structures by Bazylenko and Gross¹³ although the process conditions (hollow cathode discharge plasma source using a mixture of CF_4/CHF_3 , Ar or O_2) used were different from those in the current study. It appears that the presence of the layer of photoresist on the metal mask is responsible for a better edge profile under the conditions described in this article. This is particularly important because it could be the basis of a cost-effective method of fabricating $0\text{--}5\ \mu\text{m}$ deep devices with sharp edges and near vertical walls using RIE.

The question of how or if the thickness of the photoresist influences the shape of the edge profile, now under investigation, is not yet fully understood. However, in the present work, we have anticipated that photoresist as a dielectric material would allow a more uniform distribution of the electrical field on the surface of the sample during the etching process and prevent erosion of the edges. The possible presence of thin native oxide or of that produced at the surface of the nickel layer by interaction with oxygen plasma (CF_4/O_2) can affect the conductivity of the mask material during the etching process. This oxide, to some degree, may affect the roughness induced beneath the mask by virtue of creating an artificial dielectric layer on the top of the nickel, but further study is required before a conclusion can be drawn. However, the conductivity should remain significantly high compared to that of photoresist since clear differences are observed between the features of specimens etched with and without photoresist covering the nickel mask (Fig. 5). Therefore, in the simulation below, we have discounted the reduction of the conductivity of nickel induced by the plasma treatment so as to model an ideal case that explains the present experimental results.

D. Simulation and masking model

The above results and discussion show that the masking techniques employed here during RIE are important factors that significantly influence the profile of the etched features. In order to quantitatively understand this effect in greater detail we have simulated the electric field distribution around the edges of the mask material by solving either the Laplace equation (for metallic substrates) or the Poisson equation for dielectric substrates. The model consists of estimating the

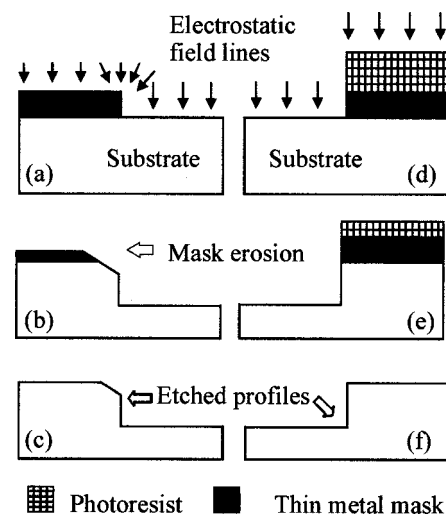


FIG. 6. Phenomenological etching model showing the etching mechanism for samples coated with a thin metal mask (a)–(c) and samples with a dielectric layer on the top of the metallic mask (d)–(f).

local electric field and comparing it to the macroscopically applied electric field. The ratio between these two quantities is the field enhancement factor, β , for the two identically geometric square substrates of metal and a dielectric with $\epsilon_r=5$. It was found that at the corner of the dielectric substrate the maximum value of β obtained was 1.25, whereas the field enhancement at the corner of the metallic substrate is 1.75. Enhancements above 1 at the corner can be attributed to the apex of the corners and the higher value in the metallic case can be attributed to the higher conductivity of the material and lower field penetration into the metal. Consequently the ion yield will be larger at the edges of the metallic mask than at the dielectric mask. This causes the edges of the masks to be etched away, with this effect being more pronounced in the case of the metallic masks.

The agreement between the experimental observation and the simulation, with regard to erosion of the edge of the etched walls where only a simple thin metal mask is used, allows us to propose the following phenomenological model of metal mask erosion during a RIE process. For a thin, uncoated metal mask there is higher field enhancement during the RIE process at the exposed edges of the mask that induces erosion of the metal mask at these points [Fig. 6(a)]. The mask will slowly be etched back, progressively exposing more of the substrate to the ion flux. The result of this process is that the edge of the etched wall will have an eroded appearance, as shown in Figs. 6(b) and 6(c) and not an ideal perpendicular profile. One way of addressing this effect is to spin coat an additional layer of dielectric onto the metallic mask which would lead to a more uniform distribution of the electrical field at the surface of the specimen [Fig. 6(d)]. This would prevent the mask from being etched back while the photoresist coating is still present, resulting in a better edge profile [Figs. 6(e) and 6(f)]. The redeposition of nonvolatile material that occurs during the etching process could compromise the etch rate, sharpness and roughness of the final etched surface and is the subject of further study.

IV. CONCLUSION

The etch rate of Pyrex (95 nm/min) in the rf/ μ w-RIE system studied here is high compared to that published using conventional RIE systems and is sufficient for the fabrication of features with depths up to 15 μ m. The etching is dependent on many process parameters, such as the rf induced self-bias, microwave power, process pressure, gas composition, etc. The most dramatic effect was found by substituting CF₄/O₂ for CF₄/Ar as the feed gas. In almost identical experimental conditions, the etch rate of a CF₄/O₂ plasma is 1.5 times higher than that of a CF₄/Ar plasma. Also, CF₄/O₂ plasma produces a smoother etched surface, has a higher etch rate and avoids roughening of the masked areas, which is observed when using CF₄/Ar for the material used here.

The observed roughening of the sample through a thin metal mask for the CF₄/Ar gas mixture is believed to be due to the Ar ions having sufficient kinetic energy to cause cratering or etching of the substrate below the mask. AFM analysis of the reactive ion etched metal masked Pyrex samples showed that there was erosion of the edge profile between the unetched surface and the etched wall. A simulation was used to show an enhancement of the electrostatic field at the edges of the thin metallic mask which was less significant for the dielectric coated mask. Therefore, it was suggested that this enhanced field would cause the edge of the mask to be preferentially etched. A phenomenological model was proposed to explain this and a simple technique

involving use of a dielectric coated metal mask was proposed and shown to overcome this problem for deep etching up to 15 μ m. This technique resulted in the fabrication of structures with improved sidewalls and highly defined edges.

ACKNOWLEDGMENTS

The authors wish to acknowledge the financial support of the UK Engineering and Physical Sciences Research Council (EPSRC). This work was part of a project in collaboration with the University of Kent, Canterbury, UK.

- ¹C. Peirrat, T. Siegrist, J. De Marco, L. Harriot, and S. Vaida, *J. Vac. Sci. Technol. A* **14**, 63 (1996).
- ²M. Esashi, *Microsyst. Technol.* **1**, 2 (1994).
- ³K. D. Skeldon, J. Mackintosh, M. von Gradowski, S. Thieux, and R. Lee, *J. Opt. A, Pure Appl. Opt.* **3**, 183 (2001).
- ⁴N. St. J. Braithwaite, *Plasma Sources Sci. Technol.* **9**, 517 (2000).
- ⁵P. W. Leech, *Vacuum* **55**, 191 (1999).
- ⁶X. Li, T. Abe, and M. Esashi, *Sens. Actuators A* **87**, 139 (2001).
- ⁷S. Rauf and M. Kushner, *IEEE Trans. Semicond. Manuf.* **11**, 486 (1998).
- ⁸H. Ito and N. Sakudo, *Ion Implantation Technology-96*, IEEE, 1997, p. 291.
- ⁹R. D'Agostino, F. Cramarossa, S. De Benedictis, and G. Ferraro, *J. Appl. Phys.* **52**, 1259 (1981).
- ¹⁰E. W. Berg and S. W. Pang, *J. Vac. Sci. Technol. B* **16**, 3359 (1998).
- ¹¹Z.-H. Liu, N. M. D. Brown, and A. McKinley, *Appl. Surf. Sci.* **108**, 319 (1997).
- ¹²D. X. Ma, T. R. Webb, A. Zhao, Z. Huang, D. Tajima, and P. K. Loewenhardt, *Proceedings of the 11th ISPP Conference* (The Electrochem. Society, Pennington, NJ, 1996), p. 250.
- ¹³M. V. Bazylenko and M. Gross, *J. Vac. Sci. Technol. A* **14**, 2994 (1996).